Hindawi
Shock and Vibration
Volume 2021, Article ID 2095350, 14 pages
https://doi.org/10.1155/2021/2095350

*Research Article*

# Simulation Analysis and Experiment Research on Hydro-Pneumatic ISD Suspension

**Xiao-Liang Zhang**,[1] **Juchao Liu**,[1] **Jiamei Nie**,[2] **Hao Wei**,[2] **and Long Chen**[1]

[1]*Automotive Engineering Research Institute, Jiangsu University, 301 Xuefu Road, Zhenjiang 212013, China*
[2]*School of Automotive and Traffic Engineering, Jiangsu University, 301 Xuefu Road, Zhenjiang 212013, China*

Correspondence should be addressed to Xiao-Liang Zhang; zxl1979@ujs.edu.cn

Received 30 June 2021; Accepted 15 October 2021; Published 3 November 2021

Academic Editor: Marcos Silveira



To address the problems of mechanical two-stage inerter-spring-damper (ISD) suspension such as excessive suspension elements, complex structure, and problematic engineering implementation, a hydro-pneumatic two-stage ISD suspension, which integrates hydro-pneumatic spring and inerter, is proposed. The full vehicle model of hydro-pneumatic ISD suspension is established based on the AMESim. Simulation analysis is performed to demonstrate the effectiveness and performances of the proposed suspension. The hydro-pneumatic ISD suspension prototype is developed and tested on four-poster tire-coupled road simulator. The results suggest that, compared with single-chamber hydro-pneumatic suspension, the hydro-pneumatic ISD one can significantly reduce the vibrations of the vehicle body and wheels, but at the expense of an excessive increase of suspension working space (SWS). In contrast, although proposed suspension is also a type of dual-chamber hydro-pneumatic one, it can not only reduce these vibrations but also downsize the SWS, which means it is the best choice for a more comfortable and safer ride.

## 1. Introduction

Traditional passive suspension is mainly composed of spring and damper, and it has little room for improvement [1–3]. In 2001, Smith developed an ideal analogy theory between mechanical and electrical systems based on the conventional analogy theory and proposed the inerter concept [4]. Vehicle suspension was first considered by Smith as a vibration isolation system employing inerters, and a few suspensions with inerter were therefore developed by Smith with different combined configurations, which have been shown to offer performance advantages over conventional passive suspensions [5–9]. Some previous researches on these suspensions highlighted that inerter can add fixed virtual mass to the sprung mass to reduce sprung mass natural frequency and improve ride comfort of vehicles [10–14]. The inerter-spring-damper (ISD) suspension proposed by Smith is a breakthrough in further improving the performance of the spring-damper suspension, which is based on the classical vibration isolation theory [4, 15–20].

Zhang proposed a two-stage ISD suspension to realize the skyhook damper configuration passively and verified the effectiveness of the implementation scheme through simulation and bench test [21, 22]. The simulation and experiments in [23] proved that the mechanical two-stage ISD suspension has good performance in reducing vibration and it has potential for broad application, but the problems such as excessive suspension components and complex structure still exist.

To address the abovementioned problems, we use fusion design method to organically integrate the hydraulic inerter and the hydro-pneumatic spring to propose a two-stage ISD suspension with single structure, which is a type of dual-chamber hydro-pneumatic suspension. The proposed suspension utilizes a helical channel to connect the two chambers of dual-chamber hydro-pneumatic suspension and obtains inertance with high-speed flowing fluid between two chambers. Based on the AMESim, the full vehicle model of the hydro-pneumatic ISD suspension is established in this paper. The prototype of hydro-pneumatic ISD suspension is developed and tested on four-poster tire-coupled road

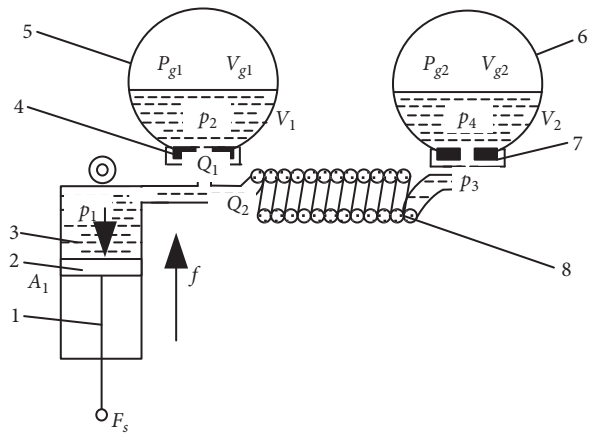


1. Piston Rod
2. Piston
3. Hydraulic cylinder
4. Damping valve I
5. Accumulator I
6. Accumulator II
7. Damper valve II
8. Helical channel

Figure 1: Schematic of hydro-pneumatic ISD suspension.

simulator to verify if the proposed ISD suspension outperforms the dual-chamber hydro-pneumatic one.

## 2. Hydro-Pneumatic Suspension Model

*2.1. Structure of Hydro-Pneumatic ISD Suspension.* The structure of the hydro-pneumatic ISD suspension based on fusion design is presented in this paper (Figure 1), and it is equipped with a damping valve at the entrance of the accumulator to suppress vibration. The piston divides hydraulic cylinder into upper and lower chambers, with the upper chamber being connected with the accumulator I and hinged with the sprung mass. The lower end of the piston rod is articulated with the unsprung mass, and the accumulator I and accumulator II are connected by a helical channel. A schematic diagram of single- and dual-chamber hydro-pneumatic suspension is provided for reference in Figure 2.

For hydro-pneumatic ISD suspension, the helical channel serves as the inertial channel where the fluid stores a large amount of kinetic energy in high-speed rotation. The difference in effective circulation areas between the helical channel and the hydraulic cylinder has an amplifying effect on fluid inertance. The nitrogen in the accumulator serves as an elastic medium and its compression can store elastic potential energy, which replaces the traditional spring. Besides, in the accumulator attachment, the damper is replaced by a throttling hole. Eventually, the hydro-pneumatic ISD suspension effectively integrates the inerter, spring, and damper organically through the medium of fluid.

*2.2. Full Vehicle Model of Hydro-Pneumatic ISD Suspension.* In this section, a full vehicle model equipped with a hydro-pneumatic ISD suspension model is established based on the AMESim (Figure 3), and its equivalent simplified model is shown in Figure 4, the following models are included, namely, chassis, hydro-pneumatic ISD suspension system, road, tire, simplified brake, models for steering, and transmission. The road and tire models are formulated in Figure 5, and the hydro-pneumatic ISD suspension system model is visualized in Figure 6. The tire model imported by the AMESim is also linear, and we will set a threshold during the simulation and test to ensure that the tire does not lift off the ground. As for the modeling of single-chamber and dual-chamber hydro-pneumatic suspensions, it can be seen from Figure 2 that a short connection between a hydraulic cylinder and the accumulator I is selected in the hydro-pneumatic ISD model, or a helical channel is replaced with a connecting channel to realize the single-chamber and dual-chamber hydro-pneumatic suspension models, respectively, and the corresponding modules in AMESim are also used to connect them to realize the simulation model. The main parameters of vehicle model and hydro-pneumatic ISD suspension are presented in Tables 1 and 2 [24–28].

## 3. Mathematical Model of Hydro-Pneumatic ISD Suspension

*3.1. Stiffness Properties.* The stiffness properties are an important characteristic of the hydro-pneumatic spring, which refer to the relationship between the elastic force of the piston rod and the stroke of the piston relative to the hydraulic cylinder. The accumulator is the rigid element of the hydro-pneumatic suspension. The gas in the accumulator I and II is considered to be an ideal gas. The state equation of gas is as follows:

$$\begin{aligned} P_2 \cdot V_1^n &= P_{g1} \cdot V_{g1}^n, \\ P_4 \cdot V_2^n &= P_{g2} \cdot V_{g2}^n. \end{aligned} \tag{1}$$

Where $P_{g1}$, $V_{g1}$, $P_{g2}$, and $V_{g2}$ are respectively the precharge pressure and initial charging volume of accumulator I and II; $P_2$, $V_1$, $P_4$, and $V_2$ are the instantaneous gas pressure and charging volume of accumulator I and II, respectively; $P_{20}$,

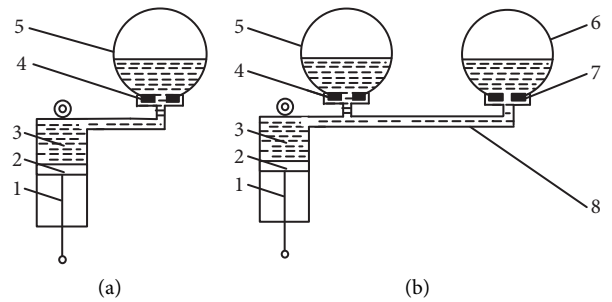


Figure 2: Schematic of (a) single-chamber and (b) dual-chamber hydro-pneumatic suspension.

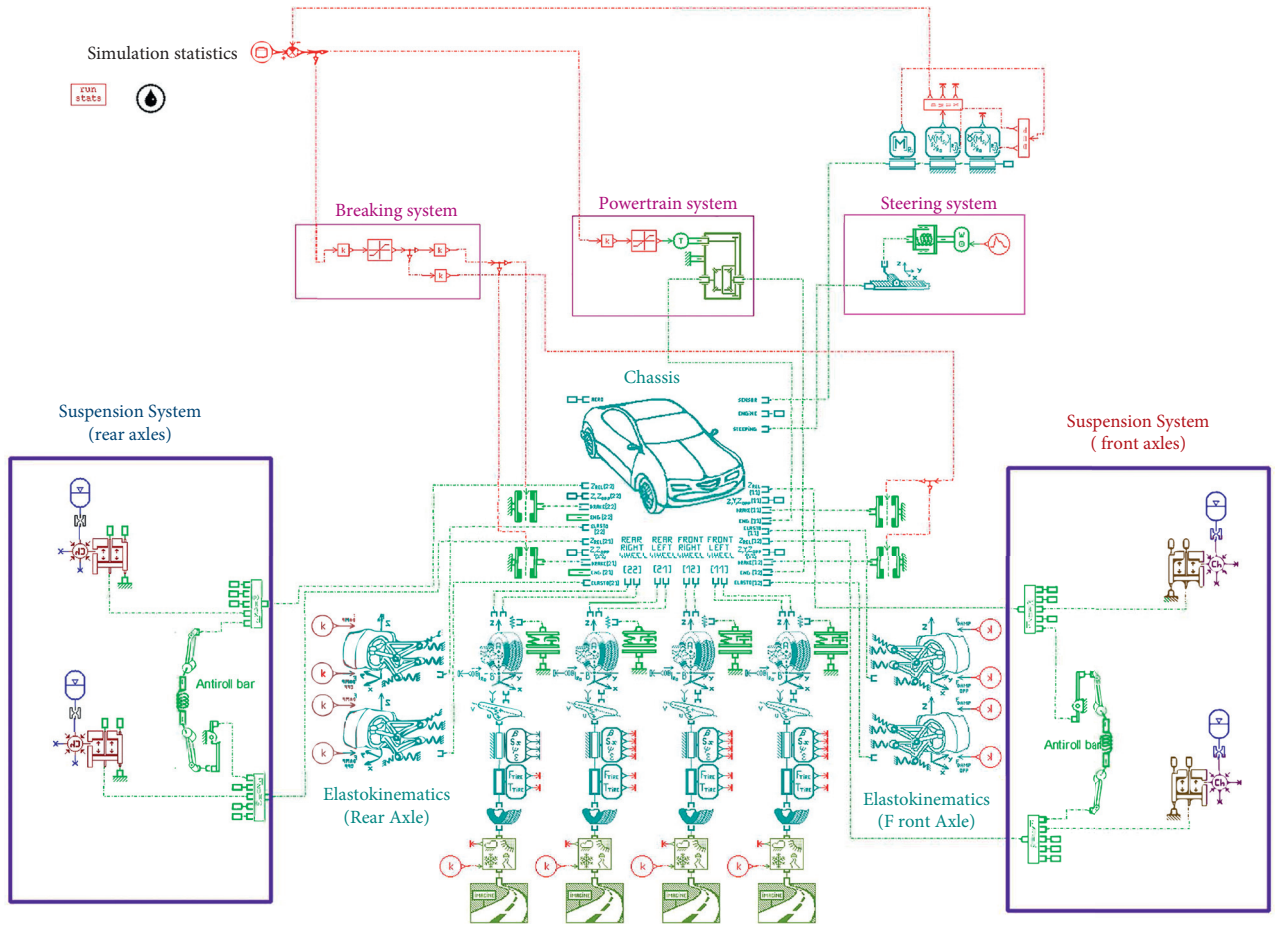


Figure 3: Vehicle dynamics model based on AMESim.

$V_{10}$, $P_{40}$, and $V_{20}$ are respectively the gas pressure and volume at the equilibrium position of accumulator I and II. It is assumed that the accumulator is an adiabatic process of ideal gas, and $n$ is the gas polytropic index, which is taken as 1.3. The change of gas volume in the accumulator can be expressed as

$$V_1 = V_{g1} + \int Q_1 \mathrm{d}t,$$
$$V_2 = V_{g2} + \int Q_2 \mathrm{d}t. \tag{2}$$

In static balance, the pressures in all parts of the hydraulic cylinder are equal, that is,

$$P_{10} = P_{20} = P_{30} = P_{40}. \tag{3}$$

*3.2. Damping Properties.* The outlets of accumulator I and II are respectively provided with damping valve I and II, as shown in Figure 1. The corresponding pressure change at both ends can be expressed as

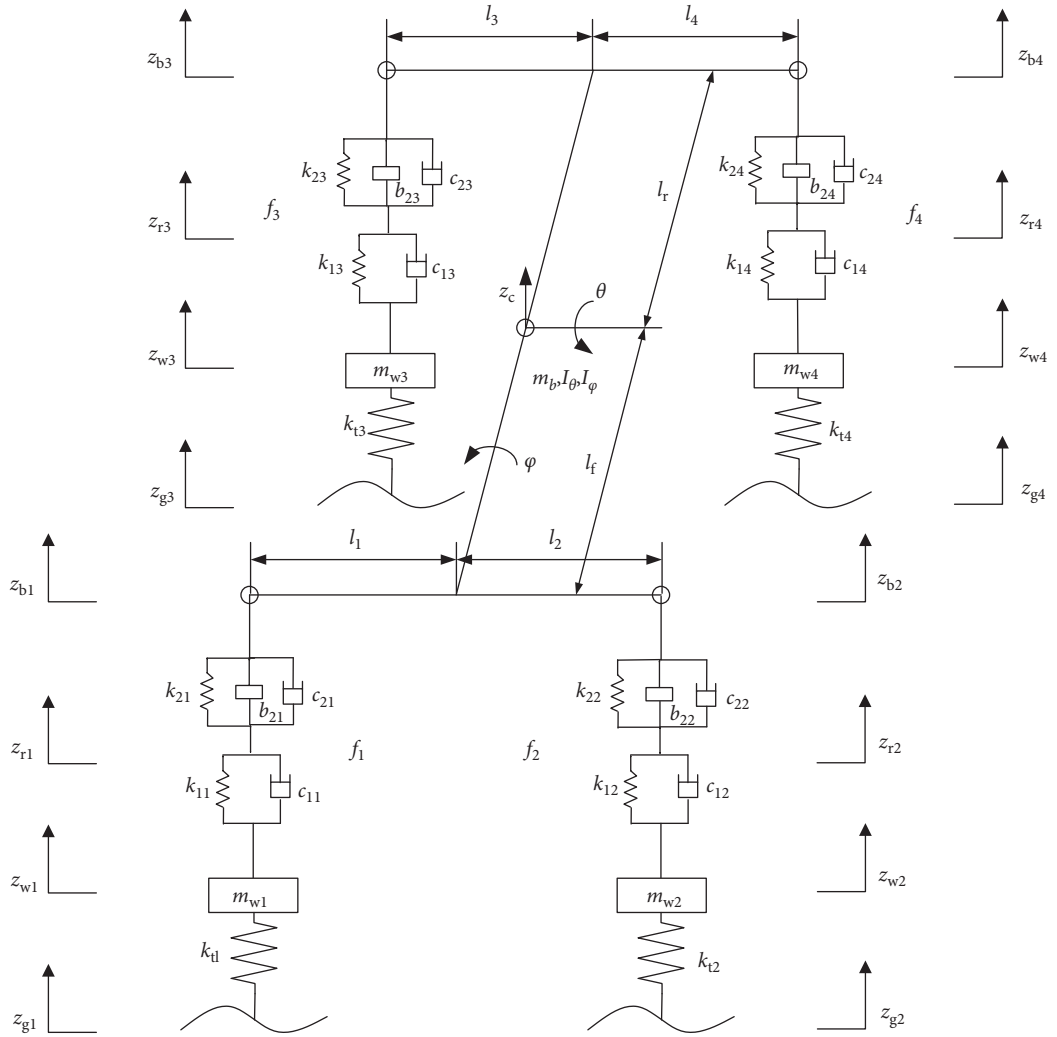


Figure 4: Equivalent simplified vehicle model.

$$P_1 - P_2 = \frac{1}{2}\rho\frac{Q_1}{C_d \cdot S_{01}} = C_1 \cdot Q_1,$$
$$P_3 - P_4 = \frac{1}{2}\rho\frac{Q_2}{C_d \cdot S_{02}} = C_2 \cdot Q_2, \tag{4}$$

where $P_1$ and $P_3$ are the pressures at the inlet of damping valve I and II, respectively, $P_2$ and $P_4$ are the pressures in accumulator I and II, respectively, $C_d$ is the flow coefficient, which is related to Reynolds number $R_e$, $S_{01}$ and $S_{02}$ are the equivalent areas of damping valve, respectively, and $\rho$ is the oil density.

*3.3. Inertance Properties.* The piston of hydro-pneumatic ISD suspension drives the high-speed fluid to move back and forth in the helical channel, stores a large amount of kinetic energy, and realizes the effect of amplifying the fluid inertance. The essential feature of hydro-pneumatic ISD suspension is that it can store and amplify the fluid inertance. However, nonlinear factors such as compressibility, viscosity, and fluid temperature still need to be considered. Combined with the hydraulic inerter structure studied [17], the inertance properties of hydro-pneumatic ISD suspension can be expressed by the fluid pressure difference at both ends of the helical channel.

$$\begin{aligned} P_1 - P_3 &= \frac{\rho \cdot l}{A_2} \cdot \dot{Q}_2 + \frac{8\mu \cdot l}{A_2 \cdot r^2} \cdot Q_2 + \frac{\rho \cdot Q_2^2}{4} + \frac{\rho \cdot Q_2^2}{2}, \\ &= \frac{\rho \cdot l}{A_2} \cdot \dot{Q}_2 + \Delta P_\mu + \Delta P_{\text{in}} + \Delta P_{\text{out}}, \end{aligned} \tag{5}$$

where $l$ is the length of helical channel, $A_2$ is the effective flow area of helical channel, $\mu$ is the fluid viscosity, and $R$ is the inner radius of the helical channel.

$\Delta P_{\text{in}}$ and $\Delta P_{\text{out}}$ are pressure losses of the inlet and outlet caused by the principle of large and small holes. By adjusting the diameter of damping valve I and II, the optimal compensation for pressure loss of the inlet and outlet can be realized. Therefore, the inertance properties can be simplified as

$$P_1 - P_3 = \frac{\rho \cdot l}{A_2} \cdot \dot{Q}_2 + \Delta P_\mu. \tag{6}$$

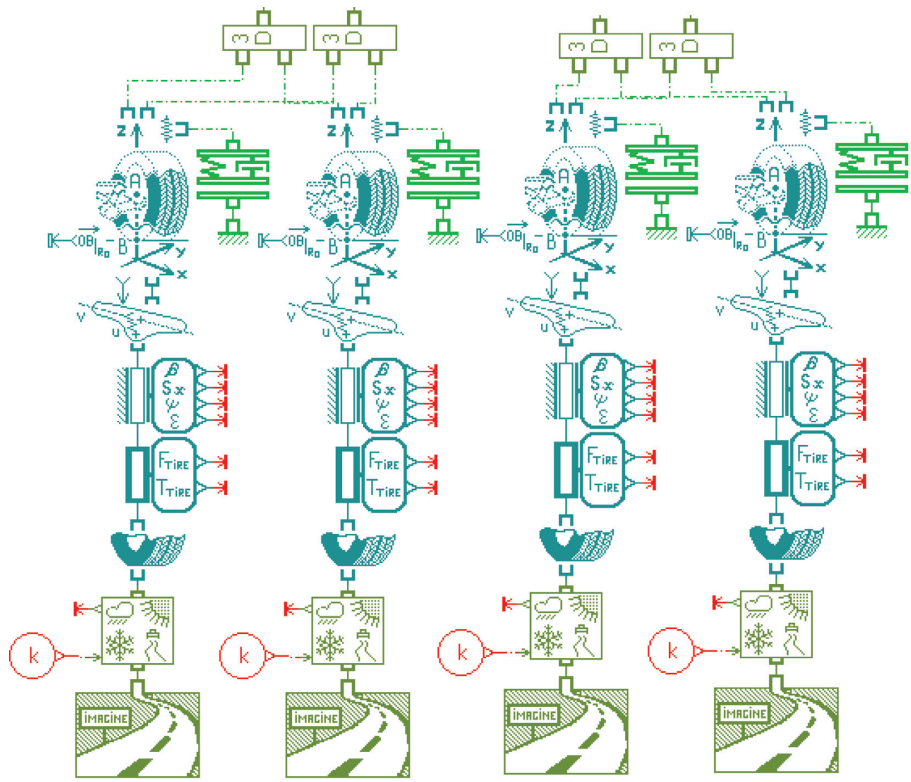


Figure 5: Road and tire model.

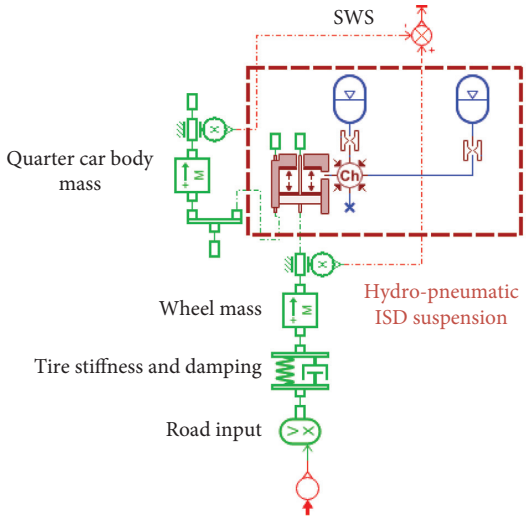


Figure 6: Hydro-pneumatic ISD suspension model.

Table 1: Main parameters of vehicle.

| Main parameters | Values |
|---|---|
| Sprung mass | 1724 kg |
| Unsprung mass of front wheel | 43.5 kg |
| Unsprung mass of rear wheel | 46.5 kg |
| Pitch moment of inertia | 2444 kg · $m^2$ |
| Roll moment of inertia | 380 kg · $m^2$ |
| Wheelbase | 2800 mm |
| Front track | 1600 mm |
| Rear track | 1600 mm |
| Distance from front axle to centroid | 1250 mm |
| Distance from rear axle to centroid | 1550 mm |
| Tire vertical stiffness | 192000 N · $m^{-1}$ |
| Tire damping | 200 N · s · $m^{-1}$ |

## 4. Simulation Analysis of Hydro-Pneumatic ISD Suspension System

*4.1. Analysis for Pulse Response.* In order to research the vibration response characteristics of the hydro-pneumatic ISD suspension under pulse input conditions, the response to a pulse excitation simulates a vehicle passing the long waveform bump. Choosing the shape of the bump to be that of a haversine of height $A = 0.1$ m and length $L = 5$ m, and with vehicle speed set at $u = 30$ km/h, this gives rise to the displacement input $q = (A/2)(1 - \cos(2\pi u/L)t)$ $(0 \le t \le (L/u))$ to the suspension.

Figure 7 and Table 3 show the time-domain response results of the system, according to which, the peak-to-peak (PTP) (the PTP values are calculated as max $(x(t))$-min $(x(t))$, where $x(t)$ are values of the signal in a period.) values of the left front/rear body acceleration (BA) and dynamic tire load (DTL) of the hydro-pneumatic ISD suspension are 19.6%, 27.0%, 27.0%, and 29.6% lower than those of the

Table 2: Hydro-pneumatic ISD suspension parameters.

| Structural parameters | Values |
|---|---|
| Number of helical channel turns | 20 |
| Hydraulic cylinder diameter | 36 mm |
| Length of helical channel | 12.68 m |
| Length of high-pressure tubing | 1.5 m |
| Diameter of damper valve I | 4 mm |
| Diameter of damper valve II | 7.6 mm |
| Inner diameter of helical channel | 6.6 mm |
| Inner diameter of helical channel device | 200 mm |
| Initial volume of front suspension accumulator I | 0.385 L |
| Initial volume of rear suspension accumulator II | 0.385 L |
| Precharge pressure of front suspension accumulator I | 42 bar |
| Precharge pressure of rear suspension accumulator I | 32 bar |
| Precharge pressure of front suspension accumulator II | 35 bar |
| Precharge pressure of rear suspension accumulator II | 25.7 bar |

single-chamber one, while the PTP values of front/rear SWS are 9.7% and 19.0% higher. While compared with the dual-chamber hydro-pneumatic suspension, the PTP values of left front/rear BA, DTL, and SWS decrease by 17.0%, 9.5%, 8.5%, 6.3%, 15.4%, and 16.5%, respectively. Therefore, the hydro-pneumatic ISD suspension can effectively suppress body vibration and improve ride comfort.

Drop I refers to the comparison between hydro-pneumatic ISD and single-chamber and can be calculated as $(S - H/S) \times 100\%$, where "$S$" and "$H$" respectively represent the values of single-chamber and hydro-pneumatic ISD. Drop II refers to the comparison of hydro-pneumatic ISD and dual-chamber and can be calculated as $(D - H/D) \times 100\%$, where "$D$" represents the values of dual-chamber. Drop I and II in Tables 4–6 are the same as this table.

*4.2. Analysis for Random Response.* To investigate the vibration response characteristics of hydro-pneumatic ISD suspension under random input conditions, the vehicle drives through a random road with a roughness coefficient of $256 \times 10^{-6} m^3$ at a speed of $u = 30$ km/h.

The simulation results are shown in Figure 8 and Table 4. Compared with the single-chamber hydro-pneumatic suspension, the RMS values of left front/rear BA and DTL of the hydro-pneumatic ISD suspension under the random road input decrease by 25.5%, 25.5%, 22.8%, and 20.8%, respectively, while the RMS values of its front/rear SWS increase by 3.0% and 3.1%, while the RMS values of left front/rear BA, DTL, and SWS decreased by 9.2%, 9.0%, 5.1%, 4.5%, 10.8%, and 9.5% compared with the dual-chamber hydro-pneumatic suspension. These prove that the hydro-pneumatic ISD suspension can effectively suppress vehicle body vibration and improve ride comfort and safety.

## 5. Bench Test System for Hydro-Pneumatic ISD Suspension

Figure 9 shows the vehicle test system for hydro-pneumatic suspensions. The rear end of vehicle is equipped with a hydraulic pump, which is connected with the hydraulic part of the hydro-pneumatic ISD suspension by a high-pressure pipeline. The charging and discharging of the hydraulic pump can adjust the height of the hydro-pneumatic ISD suspension, and the high-pressure pipeline valve can switch the hydro-pneumatic suspension in single-chamber, dual-chamber, and ISD forms. The instruments used in this bench test are shown in Table 7.

The PCB acceleration sensors used in the bench test are arranged in four positions, namely, the left front/left rear body and the left front/left rear wheel. In this way, the corresponding acceleration signals can be collected. The COMS laser displacement sensors are also installed on the left front/left rear body position, respectively, to capture signals of SWS. The S-motion speedometer is established on the right side of the vehicle body to acquire signals of the pitch and roll.

The DEWE 43A and DEWE SIRIUS are used in the data collection instrument, with the former collecting the SWS signals from the laser displacement sensor, and the latter collecting vertical acceleration signals from vehicle body/wheel and the CAN signal of S-motion. The data acquisition process is shown in Figure 10.

## 6. Test Results and Performance Analysis

*6.1. Test for Natural Frequency.* The test adopts drop method to determine the natural frequency of ISD suspension. Throughout the test, the front and rear wheels of the test vehicle are ensured to be in the center of four excitation platforms of the MTS320 tire-coupled road simulator, with the height of excitation platform being set to balance position. Then, the excitation platform is controlled to unload abruptly and descend to the position of −60 mm. Finally, the vehicle is dropped and kept free of vibration. Frequency analysis method is adopted to convert the time-domain response data into the system frequency-domain ones.

Figure 11 shows the frequency-domain response test curves of the suspension, according to which, the natural frequencies of front and rear body for the single- and dual-chamber hydro-pneumatic suspensions are 1.59 and 1.53 Hz and 1.34 and 1.36 Hz, respectively. The corresponding natural frequencies for hydro-pneumatic ISD suspension are 1.32 Hz and 1.37 Hz. Compared with the single-chamber hydro-pneumatic suspension, frequencies of the hydro-pneumatic ISD suspension have been reduced by 17.0% and 10.5%, respectively, and the peak power spectral density at the corresponding natural frequencies have been dropped by 65.4% and 61.2%, respectively. Compared with the dual-chamber hydro-pneumatic suspension, the front and rear body natural frequencies of the hydro-pneumatic ISD suspension have little change, with the peak values of the power spectral density at the corresponding natural frequency decreased by 35.5% and 31.4%, respectively. Therefore, the hydro-pneumatic ISD suspension is more beneficial in reducing the peak of the natural frequency, improving the low-frequency response and enhancing the vibration isolation performance.

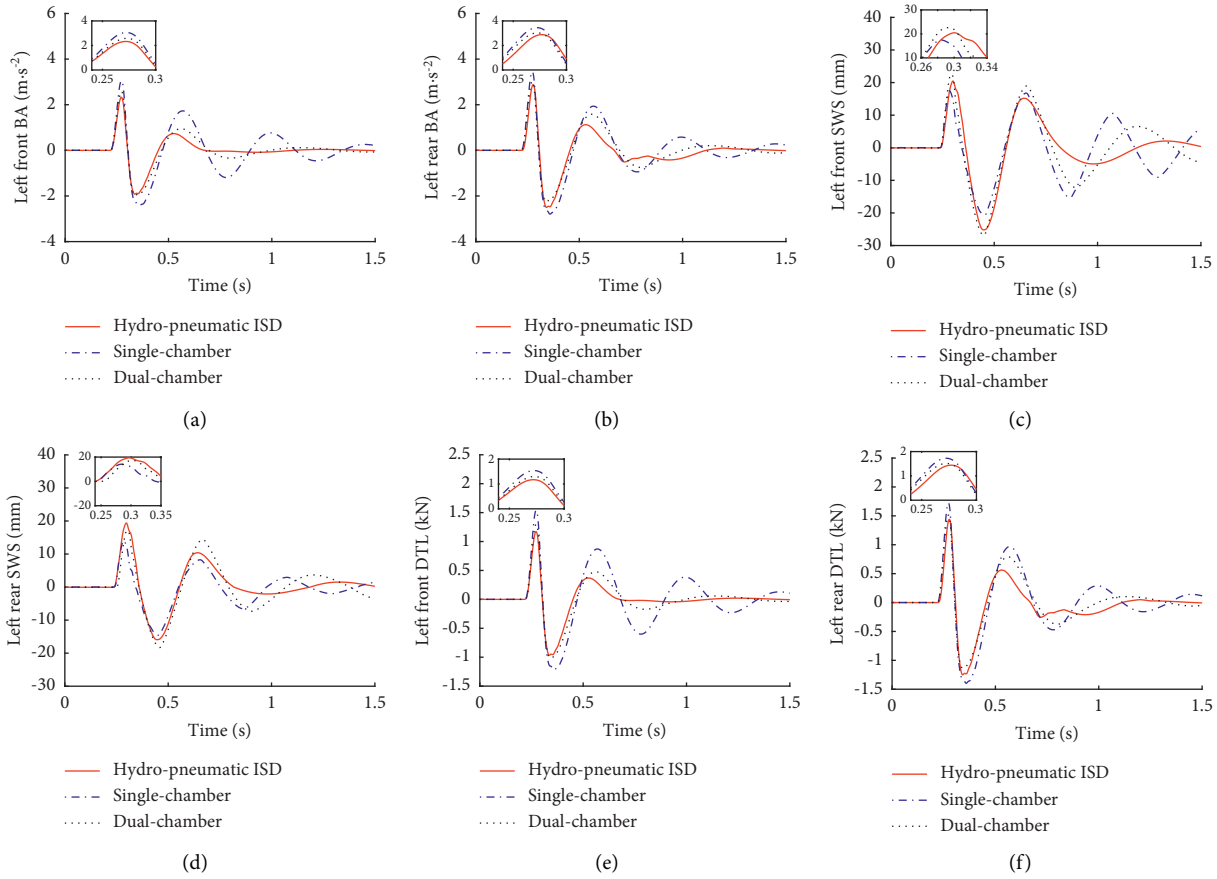


Figure 7: Comparison of pulse input response for simulation.

Table 3: PTP values of pulse input response for simulation.

| Performance index | Single-chamber | Dual-chamber | Hydro-pneumatic ISD | Drop I2 (%) | Drop II3 (%) |
|---|---|---|---|---|---|
| LF BA ($m \cdot s^{-2}$) | 6.08 | 4.89 | 4.06 | 19.6 | 17.0 |
| LR BA ($m \cdot s^{-2}$) | 6.63 | 5.38 | 4.87 | 27.0 | 9.5 |
| LF SWS (mm) | 41.25 | 49.49 | 45.27 | −9.7 | 8.5 |
| LR SWS (mm) | 28.66 | 36.40 | 34.09 | −19.0 | 6.3 |
| LF DTL (kN) | 2.86 | 2.47 | 2.09 | 27.0 | 15.4 |
| LR DTL (kN) | 3.24 | 2.73 | 2.28 | 29.6 | 16.5 |

Table 4: RMS values of random input response for simulation.

| Suspension type | LF | | | | | |
|---|---|---|---|---|---|---|
| BA ($m\ s^{-2}$) | LR | | | | | |
| BA ($m\ s^{-2}$) | LF | | | | | |
| SWS (mm) | LR | | | | | |
| SWS (mm) | LF | | | | | |
| DTL (mm) | LR | | | | | |
| DTL (mm) | | | | | | |
| Single-chamber | 1.45 | 1.49 | 2.36 | 2.28 | 5.58 | 6.16 |
| Dual-chamber | 1.19 | 1.22 | 2.56 | 2.46 | 4.83 | 5.39 |
| Hydro-pneumatic ISD | 1.08 | 1.11 | 2.43 | 2.35 | 4.31 | 4.88 |
| Drop I (%) | 25.5 | 25.5 | −3.0 | −3.1 | 22.8 | 20.8 |
| Drop II (%) | 9.2 | 9.0 | 5.1 | 4.5 | 10.8 | 9.5 |

*6.2. Test for Pulse Input.* The same pulse excitation as simulation in Section 4.1 is taken as road input for this test. The test records for the time-domain response of each signal under pulse excitation are evaluated and analyzed by calculating the peak-to-peak (PTP) value. The test results for the vehicle at the speed of $u = 30$ km/h are shown in

Table 5: PTP values of pulse input response for test.

| Performance index | Single-chamber | Dual-chamber | Hydro-pneumatic ISD | Drop I (%) | Drop II (%) |
|---|---|---|---|---|---|
| Centroid acc. (m $s^{-2}$) | 6.24 | 4.69 | 4.02 | 35.6 | 14.3 |
| LF BA (m $s^{-2}$) | 5.11 | 4.13 | 3.57 | 30.1 | 13.6 |
| LR BA (m $s^{-2}$) | 6.80 | 5.02 | 4.43 | 34.9 | 11.8 |
| LF wheel acc. (m $s^{-2}$) | 9.92 | 8.08 | 7.19 | 27.5 | 11.0 |
| LR wheel acc. (m $s^{-2}$) | 11.31 | 9.35 | 8.24 | 27.1 | 11.9 |
| LF SWS (m) | 48.30 | 63.42 | 55.46 | −14.8 | 12.5 |
| LR SWS (m) | 53.88 | 71.97 | 64.86 | −20.4 | 9.9 |
| Pitch angle (deg) | 2.83 | 3.03 | 2.70 | 4.6 | 10.9 |
| Roll angle (deg) | 2.31 | 1.98 | 1.75 | 24.2 | 11.6 |

Table 6: RMS values of random input response for test.

| Vehicle | Suspension type | Centroid acc. | | | | | | | | |
|---|---|---|---|---|---|---|---|---|---|---|
| Speed (km $h^{-1}$) (m $s^{-2}$) | LF | | | | | | | | | |
| SWS (mm) | LR | | | | | | | | | |
| SWS (mm) | LF | | | | | | | | | |
| BA (m $s^{-2}$) | LF wheel | | | | | | | | | |
| Acc. (m $s^{-2}$) | LR | | | | | | | | | |
| BA (m $s^{-2}$) | LR wheel | | | | | | | | | |
| Acc. (m $s^{-2}$) | Pitch | | | | | | | | | |
| Angle (deg) | Roll | | | | | | | | | |
| Angle (deg) [0.04em] | | | | | | | | | | |
| | Single-chamber | 1.13 | 2.23 | 1.97 | 1.58 | 42.42 | 1.50 | 36.53 | 0.16 | 0.25 |
| | Dual-chamber | 0.94 | 2.46 | 2.21 | 1.24 | 38.36 | 1.17 | 32.78 | 0.13 | 0.21 |
| 30 | ISD | 0.85 | 2.31 | 2.04 | 1.01 | 35.43 | 0.97 | 30.11 | 0.11 | 0.18 |
| | Drop I (%) | 24.8 | −3.6 | −3.6 | 36.1 | 16.5 | 35.3 | 17.6 | 31.2 | 28.0 |
| | Drop II (%) | 9.6 | 6.1 | 7.7 | 18.5 | 7.6 | 17.1 | 8.1 | 15.4 | 14.3 |
| | Single-chamber | 1.26 | 3.03 | 3.78 | 1.70 | 44.88 | 1.64 | 41.22 | 0.21 | 0.30 |
| | Dual-chamber | 1.08 | 3.31 | 4.38 | 1.35 | 40.46 | 1.28 | 37.03 | 0.17 | 0.25 |
| 40 | ISD | 0.95 | 3.13 | 4.14 | 1.13 | 37.29 | 1.06 | 34.27 | 0.15 | 0.22 |
| | Drop I (%) | 24.6 | −3.3 | −9.5 | 33.5 | 16.9 | 35.4 | 16.9 | 28.6 | 26.7 |
| | Drop II (%) | 12.0 | 5.4 | 5.5 | 16.3 | 7.4 | 17.2 | 7.5 | 11.8 | 12.0 |
| | Single-chamber | 1.38 | 3.45 | 4.55 | 1.77 | 45.61 | 1.73 | 45.57 | 0.26 | 0.36 |
| | Dual-chamber | 1.20 | 3.99 | 5.28 | 1.42 | 41.23 | 1.41 | 41.13 | 0.22 | 0.31 |
| 50 | ISD | 1.06 | 3.73 | 4.84 | 1.16 | 38.10 | 1.18 | 37.68 | 0.19 | 0.27 |
| | Drop I (%) | 23.2 | −8.1 | −6.4 | 34.5 | 16.5 | 31.8 | 17.3 | 26.9 | 25.0 |
| | Drop II (%) | 11.7 | 6.5 | 8.3 | 18.3 | 7.6 | 16.3 | 8.4 | 13.6 | 12.9 |

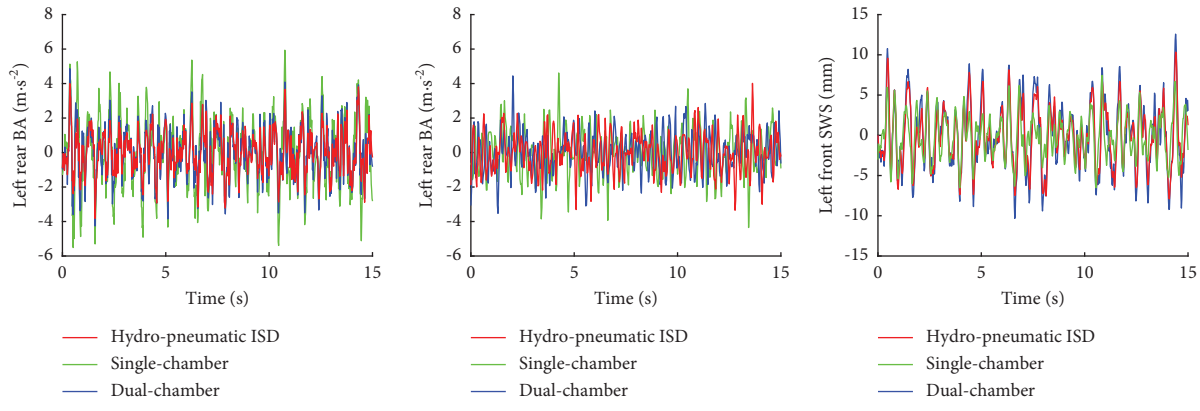


Figure 8: Continued.

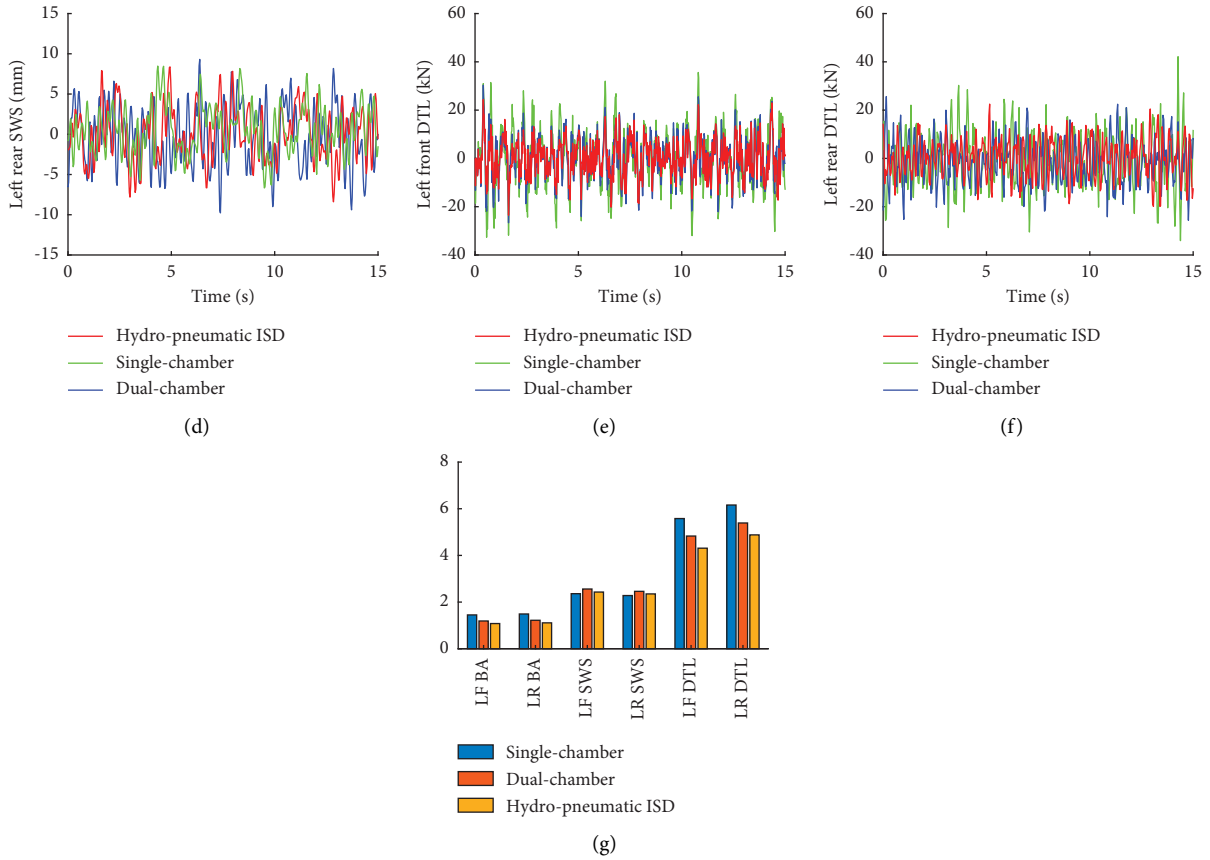


Figure 8: Comparison of random input response for simulation.


Figure 9: Vehicle test system for hydro-pneumatic suspensions.

Table 7: Test instruments.

| Instrument | Factory | Model | Precision/sensitivity | Range | Number |
|---|---|---|---|---|---|
| Acceleration sensors | PCB | 33B30 | 1% | 5000 g | 4 |
| DEWE dynamic signal analyzer | Kistler | 43A | 1 $\mu$s | 10 v | 1 |
| DEWE dynamic signal analyzer | Kistler | SIRIUS | 1 $\mu$s | 10 v | 1 |
| CMOS laser displacement sensor | KEYENCE | IL300 | 30 $\mu$m | 290 mm | 2 |
| S-motion speedometer | Kistler | CSMOTA | 0.1% | 4 g | 1 |

Figure 12, and the PTP values of test are presented in Table 5.

These results show that compared with the single-chamber hydro-pneumatic suspension, the PTP values of pitch/roll angle and of vertical acceleration for the left front/rear wheel, the left front/rear body, and the centroid of the hydro-pneumatic ISD suspension are significantly dropped by 4.6%, 24.2%, 27.5%, 27.1%, 30.1%, and 34.9%,

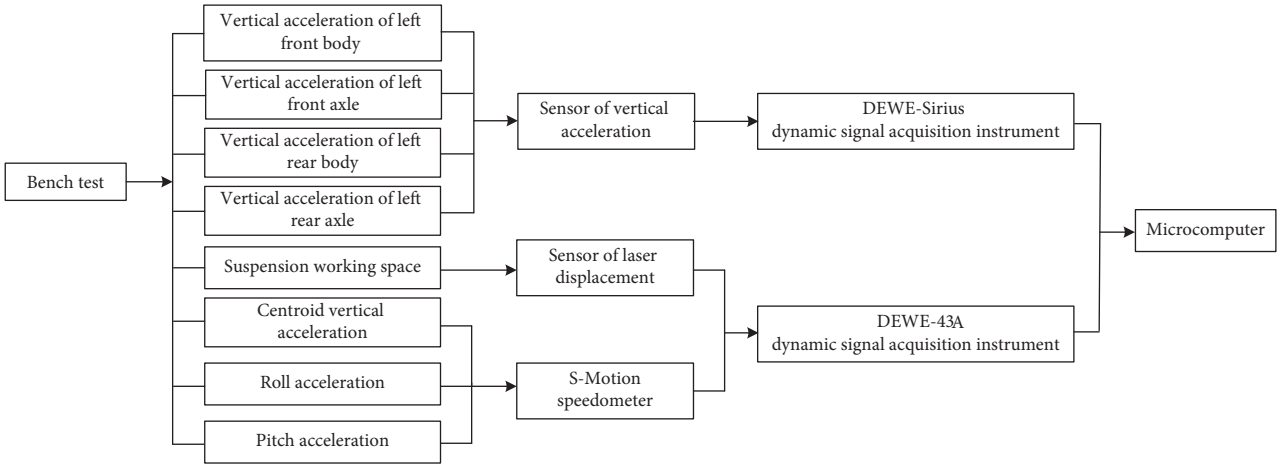


Figure 10: Schematic of data acquisition.

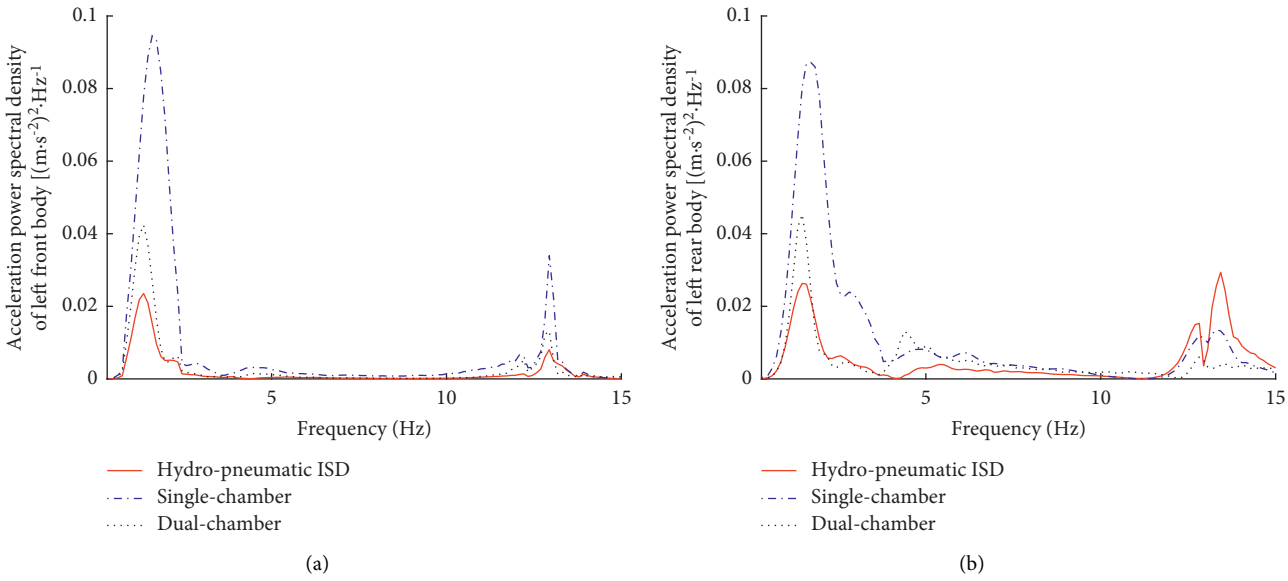


Figure 11: Comparison of natural frequency test results.

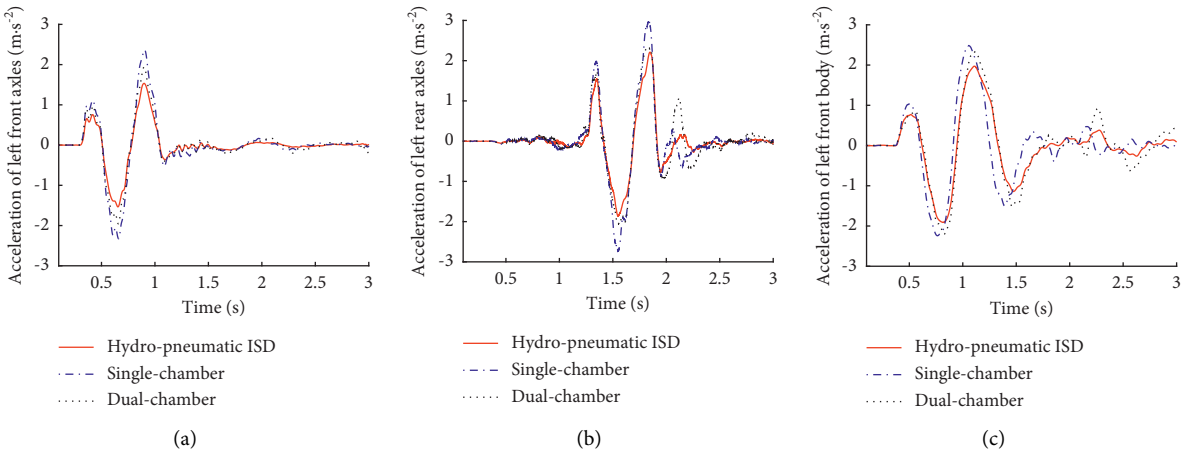


Figure 12: Continued.

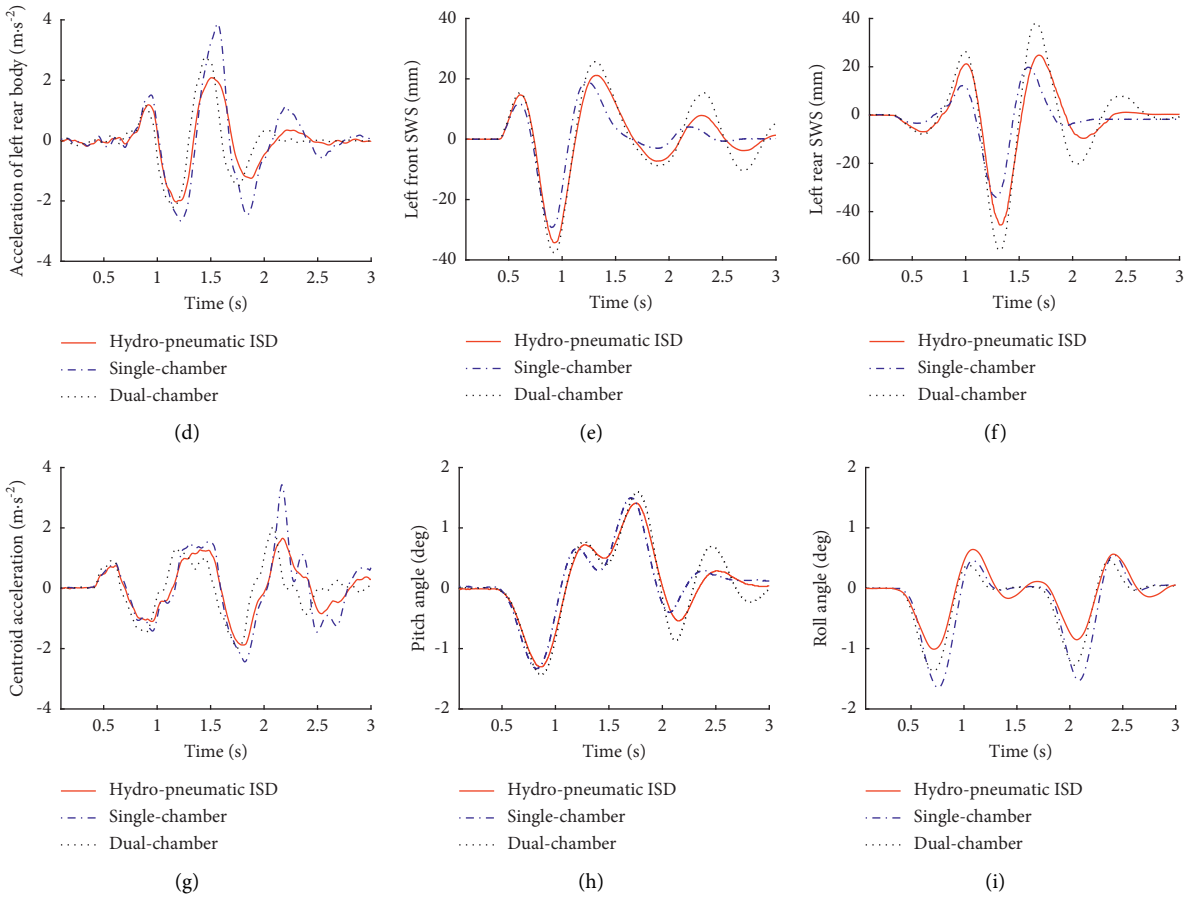


Figure 12: Comparison of pulse input test results.

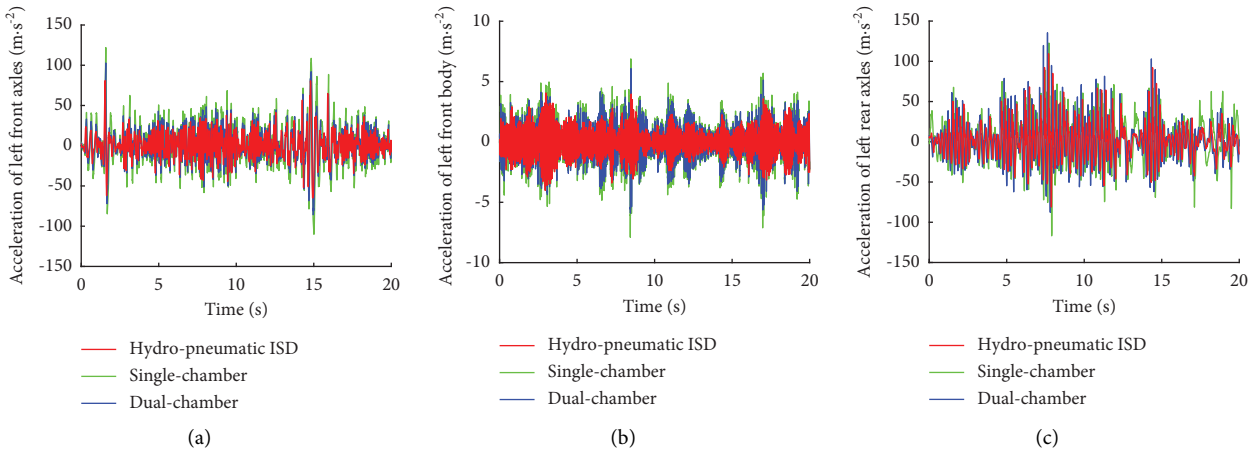


Figure 13: Continued.

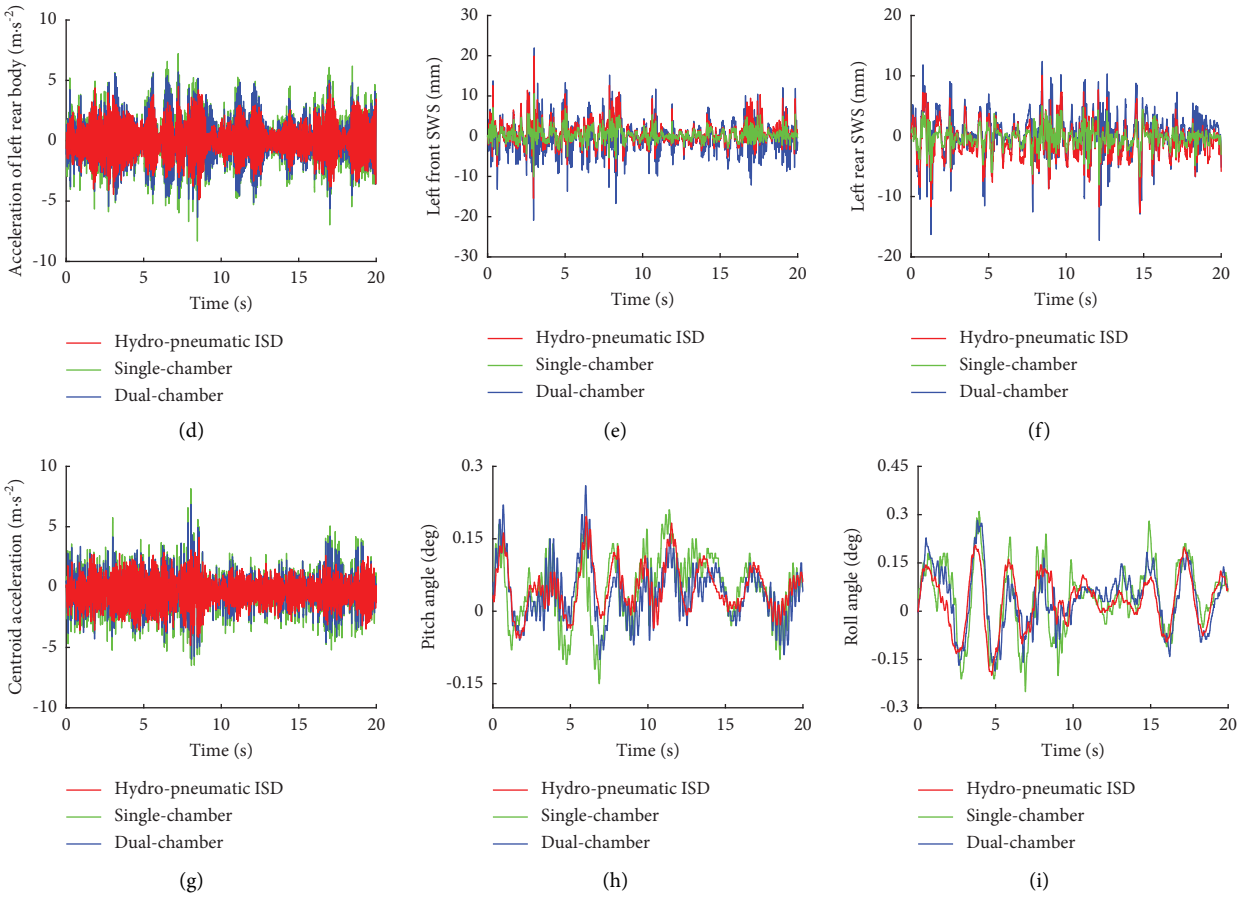


Figure 13: Comparison of random input test results.

respectively; but the PTP values of front/rear SWS increased. Compared with the dual-chamber hydro-pneumatic suspension, the corresponding PTP values of the hydro-pneumatic ISD suspension are improved by 10.9%, 11.6%, 11.0%, 11.9%, 13.6%, 11.8%, 14.3%, 12.5%, and 9.9%, respectively. Apparently, the hydro-pneumatic ISD suspension can effectively decrease the vertical vibration of the vehicle body and wheel, and it can also enhance the SWS and the overall performance of the vehicle compared with the dual-chamber hydro-pneumatic suspension.

*6.3. Test for Random Input.* In this test, the responses to random excitation simulate a vehicle traveling on a stone block pavement at the speed of 30, 40, and 50 km/h. The test results are shown in Table 6 and Figure 13.

It can be seen from Table 6 and Figure 13 that, compared with single-chamber hydro-pneumatic suspension, the RMS values of acceleration for the centroid, left front/left rear body, body pitch, and body roll of the hydro-pneumatic ISD suspension at the speed 30, 40, and 50 km/h are all reduced to different degrees with the maximum reduction reaching 35.3%, 35.4%, and 34.5%, respectively; only the RMS values of the left front/left rear SWS have a slight increase. These prove that hydro-pneumatic ISD suspension can effectively suppress vertical, pitch, and roll vibration of the body compared with single-chamber one. Moreover, the hydro-pneumatic ISD suspension can decrease vibration of the wheel, which can reflect road holding of a vehicle [29]; however, the SWS gets worse.

Observe from Table 6 and Figure 13 that compared with the dual-chamber hydro-pneumatic suspension, the RMS values of the hydro-pneumatic ISD suspension at the speed 30, 40, and 50 km/h are decreased by different degrees, with the maximum drop of 18.5%, 17.2%, and 18.3%, respectively. It turns out the hydro-pneumatic ISD suspension can effectively suppress vertical, pitch, and roll vibration of the body and also decrease the SWS to improve ride comfort and safety of the vehicle.

## 7. Conclusions

(1) The full vehicle model of the hydro-pneumatic ISD suspension is established based on AMESim to investigate the performance differences between the hydro-pneumatic ISD suspension and the single-/dual-chamber hydro-pneumatic suspension. The simulation results suggest that the hydro-pneumatic ISD suspension can effectively decrease the vibration of vehicle body and SWS, thus improving driving comfort and safety compared with dual-chamber hydro-pneumatic suspension.

(2) The hydro-pneumatic ISD suspension test prototype was designed and developed, which is installed on

the vehicle bench, and a bench test is carried out on the four-poster tire-coupled road simulator. The results show that, compared with the single-chamber hydro-pneumatic suspension, the hydro-pneumatic ISD one can significantly reduce the vibration of vehicle body and wheels, but it would remarkably increase the working space of suspension. Compared with the dual-chamber hydro-pneumatic suspension, the hydro-pneumatic ISD one can not only decrease the vibration of vehicle body and wheels but also reduce the working space of suspension. Thus, it can make driving much more comfortable and safe, and it has the potential to be used as an alternative technical scheme of dual-chamber hydro-pneumatic suspension. In the next research work, we will conduct road tests on real vehicles to check its comprehensive performance and lay the foundation for future applications in vehicles.

## Data Availability

The data used to support the findings of this study are available from the corresponding author upon request.

## Conflicts of Interest

The authors declare that there are no conflicts of interest regarding the publication of this paper.

## Acknowledgments

This work was supported by the National Natural Science Foundation of China (Grant nos. 51875257 and 51805223) and the Jiansu Government Scholarship for Overseas Studies (Grant no. JS-2019-192).

## References

[1] I. T. Al-Zahrnah, *Performance evaluation and multiobjective optimization of passive vehicle suspension systems*, Ph.D. Thesis, King Fahd University of Petroleum & Minerals, Dhahran, Saudi Arabia, 1993.

[2] P. J. T. Venhovens, "The development and implementation of adaptive semi-active suspension control*," *Vehicle System Dynamics*, vol. 23, no. 1, pp. 211–235, 1994.

[3] I. Martins, M. Esteves, F. P. Da Silva, and P. Verdelho, "Electromagnetic hybrid active-passive vehicle suspension system," in *Proceedings of the 1999 IEEE 49th Vehicular Technology Conference (Cat. No. 99CH36363)*, vol. 3, pp. 2273–2277, IEEE, Houston, TX, USA, May 1999.

[4] M. C. Smith, "Synthesis of mechanical networks: the inerter," *IEEE Transactions on Automatic Control*, vol. 47, no. 10, pp. 1648–1662, 2002.

[5] M. C. Smith, "The inerter: a retrospective," *Annual Review of Control, Robotics, and Autonomous Systems*, vol. 3, no. 1, pp. 361–391, 2020.

[6] X.-L. Zhang, T. Zhang, J. Nie, and L. Chen, "A semiactive skyhook-inertance control strategy based on continuously adjustable inerter," *Shock and Vibration*, vol. 2018, Article ID 6828621, 8 pages, 2018.

[7] D. J. Wagg, "A review of the mechanical inerter: historical context, physical realisations and nonlinear applications," *Nonlinear Dynamics*, vol. 104, no. 8, 2021.

[8] Y. Shen, J. Z. Jiang, S. A. Neild, and L. Chen, "Vehicle vibration suppression using an inerter-based mechatronic device," *Proceedings of the Institution of Mechanical Engineers–Part D: Journal of Automobile Engineering*, vol. 234, no. 10-11, pp. 2592–2601, 2020.

[9] L. Yang, R. Wang, X. Meng, Z. Sun, W. Liu, and Y. Wang, "Performance analysis of a new hydropneumatic inerter-based suspension system with semi-active control effect," *Proceedings of the Institution of Mechanical Engineers–Part D: Journal of Automobile Engineering*, vol. 234, no. 7, pp. 1883–1896, 2020.

[10] L. Yang, R. Wang, R. Ding, W. Liu, and Z. Zhu, "Investigation on the dynamic performance of a new semi-active hydro-pneumatic inerter-based suspension system with mpc control strategy," *Mechanical Systems and Signal Processing*, vol. 154, Article ID 107569, 2021.

[11] T. D. Lewis, J. Z. Jiang, S. A. Neild, C. Gong, and S. D. Iwnicki, "Using an inerter-based suspension to improve both passenger comfort and track wear in railway vehicles," *Vehicle System Dynamics*, vol. 58, no. 3, pp. 472–493, 2020.

[12] X. Yang, L. Yan, Y. Shen, H. Li, and Y. Liu, "Dynamic performance analysis and parameters perturbation study of inerter–spring–damper suspension for heavy vehicle," *Journal of Low Frequency Noise, Vibration and Active Control*, vol. 40, p. 1461348420962898, 2020.

[13] Z. Zhu, R. Wang, L. Yang, Z. Sun, and X. Meng, "Modelling and control of a semi-active dual-chamber hydro-pneumatic inerter-based suspension system," *Proceedings of the Institution of Mechanical Engineers–Part D: Journal of Automobile Engineering*, 2021.

[14] Y. Wang, H. Ding, and L. Q. Chen, "Averaging analysis on a semi-active inerter–based suspension system with relative-acceleration–relative-velocity control," *Journal of Vibration and Control*, vol. 26, no. 13-14, pp. 1199–1215, 2020.

[15] M. C. Smith and F.-C. Wang, "Performance benefits in passive vehicle suspensions employing inerters," *Vehicle System Dynamics*, vol. 42, no. 4, pp. 235–257, 2004.

[16] S. J. Swift, M. C. Smith, A. R. Glover, C. Papageorgiou, B. Gartner, and N. E. Houghton, "Design and modelling of a fluid inerter," *International Journal of Control*, vol. 86, no. 11, pp. 2035–2051, 2013.

[17] X.-L. Zhang, C. Geng, J.-M. Nie, and Q. Gao, "The missing mem-inerter and extended mem-dashpot found," *Nonlinear Dynamics*, vol. 101, no. 2, pp. 835–856, 2020.

[18] F.-C. Wang and W.-J. Su, "Impact of inerter nonlinearities on vehicle suspension control," *Vehicle System Dynamics*, vol. 46, no. 7, pp. 575–595, 2008.

[19] M. F. Soong, R. Ramli, and W. N. L. Wan Mahadi, "Ride evaluation of vehicle suspension employing non-linear inerter," *Applied Mechanics and Materials*, vol. 471, pp. 9–13, 2013.

[20] A. Martini, G. Bellani, and C. Fragassa, "Numerical assessment of a new hydro-pneumatic suspension system for motorcycles," *International Journal of Automotive and Mechanical Engineering*, vol. 15, no. 2, 2018.

[21] X. L. Zhang, J. J. Liu, J. M. Nie, and L. Chen, "Design principle and method of a passive hybrid damping suspension system," *Applied Mechanics and Materials*, vol. 635-637, pp. 1232–1240, 2014.

[22] L. Chen, X. L. Zhang, J. M. Nie, H. B. Jiang, and R. C. Wang, "Passive skyhook and ground damping vibration isolation system," *US Patent No*, vol. 9, no. 074, p. 652, 2015.
[23] Z. Xiaoliang, C. Long, N. Jiamei, W. Ruochen, and C. Yuexia, "Analysis and experiment of frequency response characteristics of two-stage series-connected isd suspension," *Journal of Jiangsu University*, vol. 33, no. 3, pp. 255–258, 2012.
[24] Z. Xiaoliang, Z. Huaxin, and J. Tao, "Vehicle road test of isd suspension with inerter and damper connected in series," *Automotive Engineering*, vol. 11, 2016.
[25] L. Chen, "Performance analysis of two-stage series-connected inerter-spring-damper suspension based on half-car model," *Journal of Mechanical Engineering*, vol. 48, no. 6, p. 102, 2012.
[26] Automobiles citroen presentation c5, https://www.leschroniquesdegoliath.com/wp-content/uploads/2018/01/Revue-technique-Citroen-C5-Fr.pdf, 2000.
[27] Z. L. Zhang, G. Q. Meng, and R. Q. Dai, "The simulation and analysis of hydro-pneumatic suspension performance based on amesim," *Advanced Materials Research*, vol. 772, pp. 416–421, 2013.
[28] N. M. Ghazaly and A. O. Moaaz, "Hydro-pneumatic passive suspension system performance analysis using amesim software," *International Journal of Vehicle Structures & Systems*, vol. 12, no. 1, 2020.
[29] D-w. Liu and J. Chen, "Test on random dynamic load of vehicle on road surface," *Journal of agricultural machinery*, vol. 36, no. 7, pp. 12–14, 2005.